Enabling mURLLC Under $\kappa - \mu$ Shadowed Fading by Cell-Free mMIMO

Biru Zhang[1], Qingqin Xu[1], Yuting Zhang[2], and Jie Zeng[2,3(✉)]

[1] School of Communications and Information Engineering, Chongqing University of Posts and Telecommunications, Chongqing 400065, China
{s220132211,s210131272}@stu.cqupt.edu.cn

[2] School of Cyberspace Science and Technology, Beijing Institute of Technology, Beijing 100081, China
1120200732@bit.edu.cn

[3] Department of Electronic Engineering, Tsinghua University, Beijing 100084, China
zengjie@tsinghua.edu.cn

Abstract. It is challenging to meet the requirement for massive ultra-reliable low-latency communications (mURLLC) under complex environments as well as diverse fading channels in the sixth-generation (6G) mobile communication system. In the 6G, user-centered cell-free (CF) architecture equipped with massive multiple input multiple output (mMIMO) technology breaks through the traditional cellular system design concept and is a promising research direction. Based on the CF mMIMO uplink system, we investigate how to implement mURLLC. Firstly, we use the least-squares estimation (LSE) method for channel estimation and obtain the channel estimation matrix which is utilized for obtaining user's post-processing signal-to-noise ratio (PPSNR) under $\kappa-\mu$ shadowed fading. Secondly, we deduce the probability density function (PDF) of PPSNR. Lastly, an expression for the relationship between the length of pilots (LoP) and the error probability (EP) is available using the information theory of the finite blocklength (FBL). Furthermore, for a given delay condition, we apply the golden section search algorithm (GSSA) to find the optimal LoP. The results of the simulations demonstrate that when the system is configured with appropriate parameters, the mURLLC will be enabled. Moreover, the $\kappa - \mu$ shadowed fading model can characterize almost all classic fading models.

Keywords: cell-free (CF) · massive multiple input multiple output (mMIMO) · massive ultra-reliable low-latency communications (mURLLC) · golden section search algorithm (GSSA) · $\kappa - \mu$ shadowed fading · least-squares estimation (LSE)

This work was supported by the National Natural Science Foundation of China under grant 62001264, the Fundamental Research Funds for the Central Universities, and the Beijing Institute of Technology Research Fund Program for Young Scholars.

F. Gao et al. (Eds.): Chinacom 2023, LNICST 590, pp. 447–458, 2024.
https://doi.org/10.1007/978-3-031-67162-3_28

1 Introduction

A common application scenario for the fifth-generation (5G) mobile communication system is ultra-reliable low-latency communications (URLLC). There has a number of requirements, with the uplink (UL) latency restricted to less than 0.5 ms and the reliability expected to higher than 99.999% [1]. And then the sixth-generation (6G) mobile communication system needs to realize massive ultra-reliable low-latency communications (mURLLC), which can support accessing numerous users at the same time. Additionally, enabling latency-sensitive applications requires prioritizing massive short-packet transmissions within mURLLC. Polyanskiy *et al.* [2] proposed that the finite blocklength (FBL) information theory is able to satisfy both the demands of ultra-reliability and low latency.

Massive multiple input multiple output (mMIMO) for improving the performance and capacities of wireless communication systems has been a rather mature technology in recent years. In combination with cell-free (CF) architecture, it is expected to enable mURLLC. The CF mMIMO has the potential to emerge as a crucial technology for 6G. The main idea behind CF mMIMO is to distribute numerous access points (APs) throughout an area to support multiple single-antenna user equipments (UEs) in a coordinated manner. Nasir *et al.* [3] demonstrated the great potential of CF mMIMO system to support URLLC applications by optimizing the data speed as well as energy efficiency in the downlink system. Ngo *et al.* [4] conducted an analysis of the achievable data rate for UEs and the system throughput based on a UL CF mMIMO system, taking the effects of power control, channel estimation errors, and non-orthogonality of polit into account. In addition, it is a hot research topic how to reach the mURLLC requirements under complex environments and diverse fading channels. Under Rayleigh fading, Quoc *et al.* [5] studied the post-processing signal-to-noise ratio (PPSNR) and Zeng *et al.* [6] deduced the probability density function (PDF) of the PPSNR with linear detection. Yet, the literatures mentioned above are based on the traditional fading model which is no longer applicable to the extensive and complex 6G mobile communication. Paris *et al.* [7] proposed the $\kappa-\mu$ shadowed fading model, incorporating the effects of multipath fading, shadowing, as well as path loss to precisely depict the signal propagation in real-world environments. The model covers numerous features of channel propagation and fading including Rayleigh, Nakagami-m, Rician as well as Rician shadowed fading and so on.

To the best of our knowledge, there are few investigations of mURLLC supporting short-packet transmissions in this unified fading model. Therefore, we analyze how to realize mURLLC in $\kappa-\mu$ shadowed fading model. The key contributions of this paper are organized as below:

- For the CF mMIMO system, we derive the channel estimation matrix of the least-squares estimation (LSE) method and the PDF of PPSNR of the minimum mean squared error (MMSE) detection under $\kappa-\mu$ shadowed fading.
- For short-packet transmissions, using the information theory of the FBL, we obtain an expression for the relationship between the error probability (EP) as well as the length of pilots (LoP), likewise optimize the LoP by applying the golden section search algorithm (GSSA) to minimize EP.

The remainder of this letter will be divided as below. Section 2 presents the CF mMIMO system model. Following Sect. 3 will show the PDF of PPSNR. In Sect. 4, we calculate the EP and optimize the LoP. Section 5 will discuss the numerical simulations and analysis. The conclusion can be found in Sect. 6.

Notation: $(\bullet)^T$, $(\bullet)^H$, $[\bullet]_{lk}$ and $\mathbb{E}(\bullet)$ denote transpose, conjugate and transpose, the elements of the lth row, kth column of a matrix and expectation, respectively. $\mathbb{C}^{L\times K}$ indicates a $L \times K$ matrix with complex elements, as well as $\mathbf{I}_n$ denotes an $n \times n$ identity matrix. In addition, $\mathcal{CN}$ represents the complex Gaussian distribution.

2 System Model

The UL CF mMIMO system contains a central processing unit (CPU), K single-antenna UEs and L single-antenna APs, each linked to a CPU through backhauls, as shown in Fig. 1. It's assumed that APs and UEs are randomly distributed throughout the coverage area. Moreover, we presume that APs and UEs conform to a time division duplex (TDD) protocol, comprising of a pilot phase for channel estimation and a phase to transmit data. In addition, we let n_p represent the number of channel uses (CUs) for UL pilots training, n_d for UL data transmission, and N for the sum of CUs, i.e., $N = n_p + n_d$. Furthermore, it is assumed that any one user sends a short data packet containing D information bits via N CUs, and the transmission latency and channel bandwidth are t_{D} and B, respectively, where $N = Bt_{\mathrm{D}}$.

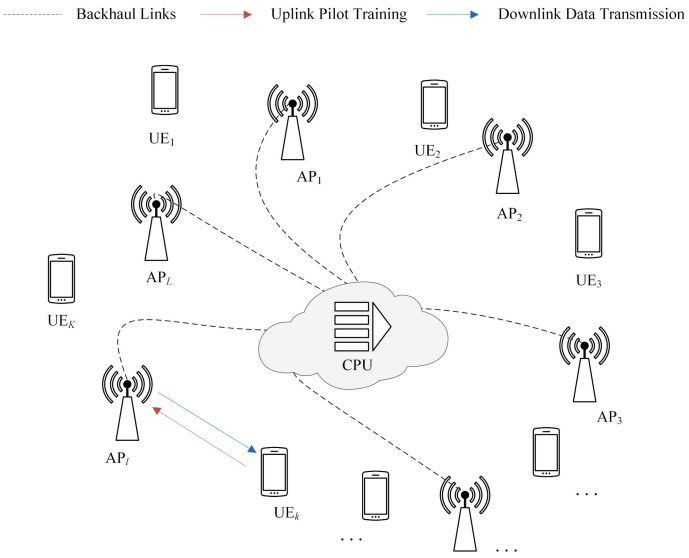

Fig. 1. The CF mMIMO system model

The channel coefficient between lth AP and kth UE can be expressed as $g_{lk} = [\mathbf{G}]_{lk} = \sqrt{\beta_{lk}} h_{lk}$, where $\mathbf{G} \in \mathbb{C}^{L \times K}$ is the channel matrix, β_{lk} is the large-scale fading coefficient [5], and h_{lk} is the small-scale and shadow fading coefficient as well as its power $|h_{lk}|^2$ is random variable (RV). For parameters m, κ and μ, the RV is expressed as [7]

$$|h_{lk}|^2 = \sum_{i=1}^{\mu} [(X_{i,lk} + \xi_{lk} p_{i,lk})^2 + (Y_{i,lk} + \xi_{lk} q_{i,lk})^2], \tag{1}$$

where $X_{i,lk}$ and $Y_{i,lk}$ are independent and identically distributed Gaussian RVs with $\mathbb{E}[X_{i,lk}] = 0$, $\mathbb{E}[Y_{i,lk}] = 0$, $\mathbb{E}[X_{i,lk}^2] = \sigma^2$ and $\mathbb{E}[Y_{i,lk}^2] = \sigma^2$; $p_{i,lk}$ and $q_{i,lk}$ are actual figures; ξ_{lk} is a Nakagami$-m$ RV whose shaping parameter is m as well as $\mathbb{E}[\xi_{lk}^2] = 1$; μ is the sum of the number of multipath clusters; $\kappa = \sum_{i=1}^{\mu} (p_{i,lk}^2 + q_{i,lk}^2)/2\mu\sigma^2$ is the ratio of the power of dominant and scattered components.

2.1 Pilot Training

We assume that the pilot training sequence by kth UE is $\boldsymbol{\varphi}_k^{n_p} = [\varphi_k^{(1)}, ..., \varphi_k^{(n_p)}] \in \mathbb{C}^{1 \times n_p}$, each designed to be orthogonal and $\|\boldsymbol{\varphi}_k^{n_p}\|^2 = 1$. Therefore, the signal received at lth AP, denoted by $\mathbf{y}_l^{n_p} \in \mathbb{C}^{1 \times n_p}$, is derived as

$$\mathbf{y}_l^{n_p} = \sqrt{n_p P_u} \sum_{k=1}^{K} g_{lk} \boldsymbol{\varphi}_k^{n_p} + \mathbf{z}_l^{n_p}, \tag{2}$$

where $\mathbf{z}_l^{n_p} \in \mathbb{C}^{1 \times n_p}$ is the noise matrix with i.i.d. elements yielding $\mathcal{CN}(0, 1)$, P_u is the average transmit power (TP) of each UE.

Based on (2), $\hat{g}_{lk}$ can be obtained by using the LSE estimation [8],

$$\hat{g_{lk}} = \frac{1}{\sqrt{n_p P_u}} \mathbf{y}_l^{n_p} (\boldsymbol{\varphi}_k^{n_p})^H = g_{lk} + w_{lk}, \tag{3}$$

where w_{lk} follows $\mathcal{CN}(0, \frac{1}{n_p P_u})$. On basis of [9], g_{lk} can also have the form of

$$(g_{lk} | \hat{g}_{lk}) = \tilde{g}_{lk} - \tilde{w}_{lk}, \tag{4}$$

where $\tilde{g}_{lk} = \sqrt{\beta_{lk}} \tilde{h}_{lk} \triangleq \Delta_k \hat{g}_{lk}$, $\Delta_k = \frac{a n_p P_u \beta_{lk}}{a n_p P_u \beta_{lk+1}}$,$a = \mathbb{E}(|h_{lk}|^2)$ and $\tilde{w}_{lk}$ follows $\mathcal{CN}(0, \frac{a \beta_{lk}}{a n_p P_u \beta_{lk+1}})$.

3 Linear Detection

In this particular section, our primary objective is to derive the PPSNR as precisely detected by utilizing the MMSE detector. Furthermore, our aim is to obtain the PDF that characterizes the distribution of the PPSNR values.

Denote $\mathbf{x}_k^{n_d} \triangleq [x_k^{(1)}, ..., x_k^{(n_d)}]^T \in \mathbb{C}^{n_d \times 1}$ as the transmit signals matrix from UE k , $\|\mathbf{x}_k^{n_d}\|^2 = 1$, and the signals received at the AP l can be given by

$$\begin{aligned}\mathbf{y}_l^{n_d} &= \sqrt{P_u}\sum_{k=1}^{K} g_{lk}\mathbf{x}_k^{n_d} + \mathbf{z}_l^{n_d} \\ &= \sqrt{P_u}\sum_{k=1}^{K}(\tilde{g}_{lk} - \tilde{w}_{lk})\mathbf{x}_k^{n_d} + \mathbf{z}_l^{n_d},\end{aligned} \tag{5}$$

where $\mathbf{y}_l^{n_d} \in \mathbb{C}^{n_d \times 1}$ and $\mathbf{z}_l^{n_d} \in \mathbb{C}^{n_d \times 1}$ is the noise matrix. By using the MMSE detector matrix [10] $\mathbf{V}_k^{\text{MMSE}} = \bar{\tilde{g}}_{lk}(\sum_{k=1}^{K}|\tilde{g}_{lk}|^2 + \frac{1}{P_u})^{-1}\mathbf{I}_{n_d}$ for user k , $\mathbf{y}_l^{n_d}$ can be used to estimate the transmit signal of user k as:

$$\begin{aligned}\mathbf{V}_k^{\text{MMSE}}\mathbf{y}_l^{n_d} &= \sqrt{P_u}v_k^{\text{MMSE}}\tilde{g}_{lk}\mathbf{x}_k^{n_d} + \sqrt{P_u}v_k^{\text{MMSE}}\sum_{j=1,j\neq k}^{K}\tilde{g}_{lj}\mathbf{x}_j^{n_d} \\ &\quad - \sqrt{P_u}v_k^{\text{MMSE}}\sum_{j=1}^{K}\tilde{w}_{lj}\mathbf{x}_j^{n_d} + v_k^{\text{MMSE}}\mathbf{z}_l^{n_d},\end{aligned} \tag{6}$$

where $v_k^{\text{MMSE}} = \bar{\tilde{g}}_{lk}(\sum_{k=1}^{K}|\tilde{g}_{lk}|^2 + \frac{1}{P_u})^{-1}$. Based on (6), the PPSNR of user k is [5]

$$\begin{aligned}\tilde{\gamma}_k(n_p) &= \frac{|v_k^{\text{MMSE}}\tilde{g}_{lk}|^2}{|v_k^{\text{MMSE}}|^2\sum_{j=1,j\neq k}^{K}|\tilde{g}_{lj}|^2 + (\sum_{j=1}^{K}\frac{a\beta_{lj}}{an_pP_u\beta_{lj+1}} + \frac{1}{P_u})|v_k^{\text{MMSE}}|^2} \\ &= \frac{\beta_{lk}|\tilde{h}_{lk}|^2}{\sum_{j=1,j\neq k}^{K}\frac{|\bar{\tilde{g}}_{lk}\tilde{g}_{lj}|^2}{|\tilde{g}_{lk}|^2} + \sum_{j=1}^{K}\frac{a\beta_{lj}}{an_pP_u\beta_{lj+1}} + \frac{1}{P_u}} = \frac{\beta_{lk}\zeta_{lk}}{\psi_j + \tilde{n}_p},\end{aligned} \tag{7}$$

where $\zeta_{lk} = |\tilde{h}_{lk}|^2$, $\tilde{n}_p = \sum_{j=1}^{K}\frac{a\beta_{lj}}{an_pP_u\beta_{lj+1}} + \frac{1}{P_u}$ and $\psi_j = \sum_{j=1,j\neq k}^{K}\frac{|\bar{\tilde{g}}_{lk}\tilde{g}_{lj}|^2}{|\tilde{g}_{lk}|^2}$.

Based on (4), since $\tilde{g}_{lk} = g_{lk} + \tilde{w}_{lk}$, $\tilde{g}_{lk} = \sqrt{\beta_{lk}}\tilde{h}_{lk}$, we can obtain $\tilde{h}_{lk} = h_{lk} + \frac{\tilde{w}_{lk}}{\sqrt{\beta_{lk}}}$. According to (1), $|h_{i,lk}|^2 = (X_{i,lk} + \xi_{lk}p_{i,lk})^2 + (Y_{i,lk} + \xi_{lk}q_{i,lk})^2$ denotes the square of the signal envelope of cluster i , and then, we can derive that $|\tilde{h}_{i,lk}|^2 = (X_{i,lk} + \text{Re}[\frac{\tilde{w}_{lk}}{\mu\sqrt{\beta_{lk}}}] + \xi_{lk}p_{i,lk})^2 + (Y_{i,lk} + \text{Im}[\frac{\tilde{w}_{lk}}{\mu\sqrt{\beta_{lk}}} + \xi_{lk}q_{i,lk})^2$. $|\tilde{h}_{lk}|^2$ can also have the form of:

$$|\tilde{h}_{lk}|^2 = \sum_{i=1}^{\mu}[(\tilde{X}_{i,lk} + \xi_{lk}p_{i,lk})^2 + (\tilde{Y}_{i,lk} + \xi_{lk}q_{i,lk})^2], \tag{8}$$

where $\tilde{X}_{i,lk} = X_{i,lk} + \text{Re}[\frac{\tilde{w}_{lk}}{\mu\sqrt{\beta_{lk}}}]$, $\tilde{Y}_{i,lk} = Y_{i,lk} + \text{Im}[\frac{\tilde{w}_{lk}}{\mu\sqrt{\beta_{lk}}}]$. Moreover, $\mathbb{E}[\tilde{X}_{i,lk}] = 0$, $\mathbb{E}[\tilde{Y}_{i,lk}] = 0$, $\mathbb{E}[\tilde{X}_{i,lk}^2] = \sigma^2 + \frac{a}{2\mu^2(an_pP_u\beta_{lk}+1)} = \tilde{\sigma}^2$ as well as $\mathbb{E}[\tilde{Y}_{i,lk}^2] = \tilde{\sigma}^2$. So, we assumed that $|\tilde{h}_{lk}|^2$ also tracks $\kappa-\mu$ shadowed distribution. From [7] and [11], the PDF of $\zeta_{lk} = |\tilde{h}_{lk}|^2$ is given by

$$f_{\zeta_{lk}}(x) = a_0x^{\mu-1} \times e^{a_1(\tilde{\kappa}\mu+m)x} \times {}_1F_1(m, \mu; -4a_1\tilde{\kappa}\mu x), \forall x > 0, \tag{9}$$

where $a_0 = \frac{m^m}{(2\tilde{\sigma}^{2\mu}\Gamma(\mu)(\tilde{\kappa}\mu+m)^m)}$, $a_1 = \frac{-1}{(2\tilde{\sigma}^2(\tilde{\kappa}\mu+m))}$, $\Gamma(\bullet)$ and ${}_1F_1(\bullet)$ are the Gamma function and the confluent hypergeometric function, respectively, and $\tilde{\kappa} = \sum_{i=1}^{\mu}(p_{i,lk}^2 + q_{i,lk}^2)/2\mu\tilde{\sigma}^2$.

To reduce the complexity of the analysis, we define $\tilde{\psi}_j = \mathrm{E}(\psi_j)$, so the PPSNR of user k can also have the form of

$$\tilde{\gamma}_k(n_p) \triangleq \frac{\beta_{lk}\zeta_{lk}}{\tilde{\psi}_j + \tilde{n}_p}. \tag{10}$$

Based on (9) and (10), the PDF of $\tilde{\gamma}_k(n_p)$ is deduced as

$$f_{\tilde{\gamma}_k}(x) = \frac{\tilde{\psi}_j + \tilde{n}_p}{\beta_{lk}} f_{\zeta_{lk}}(\frac{\tilde{\psi}_j + \tilde{n}_p}{\beta_{lk}}x)$$
$$= a_0(\frac{\tilde{\psi}_j + \tilde{n}_p}{\beta_{lk}})^{\mu}x^{\mu-1} \times e^{a_1(\tilde{\kappa}\mu+m)\frac{\tilde{\psi}_j+\tilde{n}_p}{\beta_{lk}}x} \times_1 F_1(m, \mu; -4a_1\tilde{\kappa}\mu\frac{\tilde{\psi}_j + \tilde{n}_p}{\beta_{lk}}x). \tag{11}$$

4 Formula for EP and Optimal LoP

Based on the infinite coding block length and the inapplicability of classical Shannon information theory to short packet transmissions, we use the FBL information theory to calculate an expression for the interrelation between LoP and EP, and analyze their relationship to achieve mURLLC.

In Sect. 2, it is mentioned that every user sends a short data packet containing D information bits by N CUs and $N = Bt_{\mathrm{D}}$. EP can be estimated by

$$\varepsilon(n_d, D, \gamma_k) \approx Q(\sqrt{\frac{n_d}{V(\gamma_k)}}(C(\gamma_k) - \frac{D}{n_d})), \tag{12}$$

where γ_k is the PPSNR, $V(\gamma_k) = \frac{\gamma_k(2+\gamma_k)}{[(1+\gamma_k)ln2]^2}$, $C(\gamma_k) = \frac{ln(1+\gamma_k)}{ln2}$ and $Q(t) = (\frac{1}{\sqrt{2\pi}})\int_t^{\infty}\exp(-\frac{x^2}{2})dx$.

Given t_{D} and n_p, we can combine (11) and (12) to derive the EP of user k,

$$\tilde{e}_k(n_p, t_{\mathrm{D}}) = \int_0^{\infty}\varepsilon(Bt_{\mathrm{D}} - n_p, D, x)f_{\tilde{\gamma}_k}(x)dx$$
$$= \int_0^{\infty}Q(\sqrt{\frac{Bt_{\mathrm{D}} - n_p}{V(x)}}(C(x) - \frac{D}{Bt_{\mathrm{D}} - n_p}))f_{\tilde{\gamma}_k}(x)dx. \tag{13}$$

Assuming the given t_{D}, the optimum LoP n_p^* that minimizes the EP can be determined by,

$$n_p^* = \underset{n_p\in[K, Bt_{\mathrm{D}}-1]}{\operatorname{argmin}} \tilde{e}_k(n_p, t_{\mathrm{D}}). \tag{14}$$

The GSSA [12] can be used to calculate n_p^* that is an integer according to (13). Furthermore, we can obtain the Minimum EP, $\tilde{e}_k(n_p^*, t_{\mathrm{D}})$. The specific algorithm process is shown in Fig. 2.

5 Numerical Results and Analysis

We use simulations to confirm our analysis in this section. The maximum average TP P_u is 40 dBm. The size of the short data packet information D is 40 bits. The channel bandwidth B is 1080 kHz. The specific simulation parameters are presented below in Table 1.

Table 1. Simulation Parameters

Parameter	Definition	Value
B	Bandwidth	1080 kHz
D	Packet size	40 bits
P_u	Average TP	[20 dBm, 40 dBm]
L	Amount of AP	[100, 800]
K	Amount of UE	[50, 400]

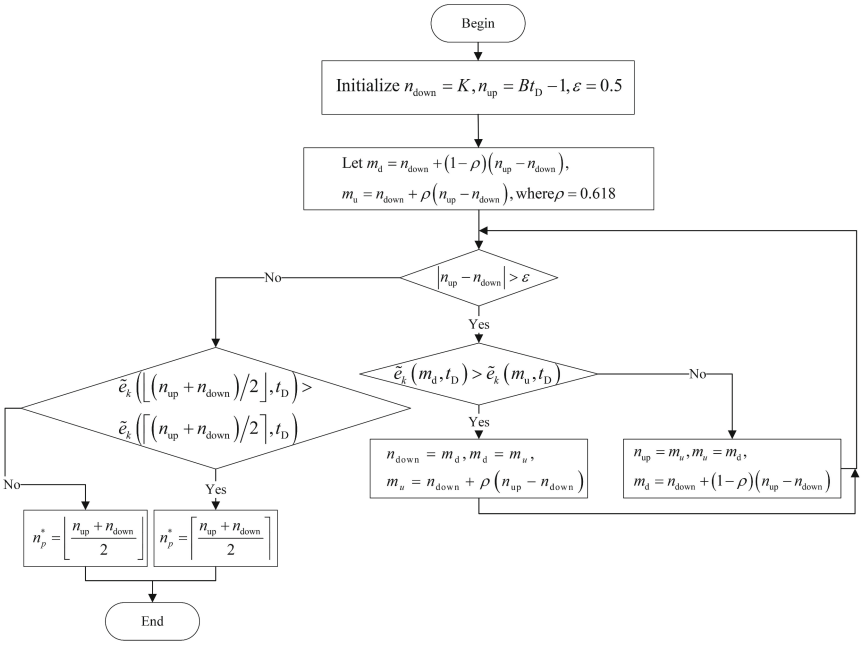

Fig. 2. The process of GSSA

Figure 3 presents the relationship between EP and t_{D} under the different fading models, when $P_u = 30$ dBm, $K = 50$ and LoP is optimal. There is a gradual increase in reliability as latency increases. With the optimal LoP, when $m = 5$, $\kappa = 4$ and $\mu = 2$ ($\kappa - \mu$ shadowed fading) as well as $m = 100$, $\kappa = 8$

and $\mu = 1$ (Rician fading) and $t_{\mathrm{D}} > 0.2$ ms, mURLLC can be enabled. It must be pointed out that adjusting the parameters such as m, κ and μ can feature fading channels that cannot be accommodated by classical models.

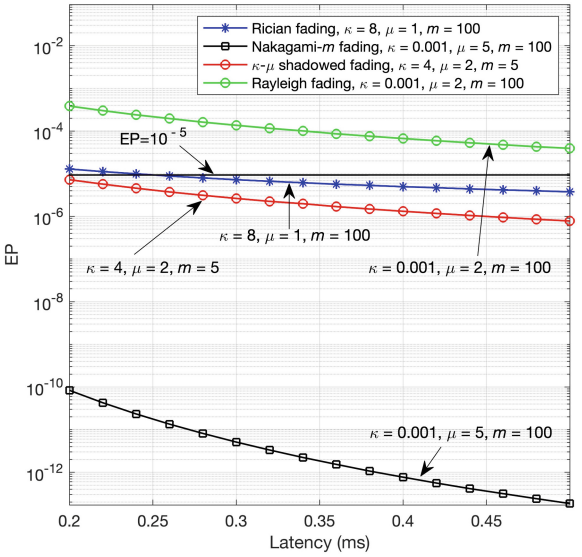

Fig. 3. EP vs. Latency: $K = 50$, $P_u = 30$ dBm

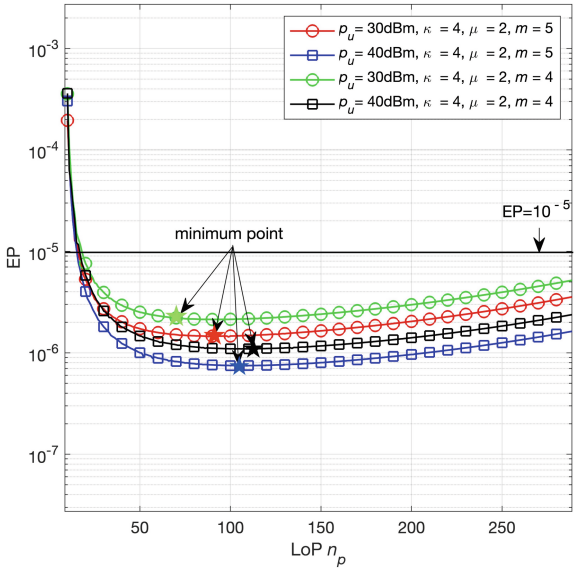

Fig. 4. EP vs. LoP n_p: $K = 50$, $t_{\mathrm{D}} = 0.5$ ms

Figure 4 illustrates the effect of the value of LoP on the EP in different TP, κ, μ and m, when $K = 50$, $t_{\mathrm{D}} = 0.5$ ms. TP are configured to be 30 dBm as well as 40 dBm individually. Simulation results well display that proper pilot lengths can reduce the EP. Moreover, the optimal LoP can be obtained by the GSSA method. As shown in the Fig. 4, when TP is 30 dBm, $m = 5$, $\kappa = 4$ and $\mu = 2$, the EP can be lowered to less than 10^{-5}, and the optimal LoP can be obtained. By comparing red curve with blue curve or comparing green curve with black curve, we can see that EP decreases with increased TP. In addition, red curve and green curve show that the EP for $m = 5$, $\kappa = 4$ and $\mu = 2$ is lower than that for $m = 4$, $\kappa = 4$ and $\mu = 2$. We note that by adjusting the values of parameters such as m, κ and μ, EP could be reduced.

Figure 5 illustrates the correlation between reliability and amount of UE under the four classical fading models, when $P_u = 30$ dBm, $t_{\mathrm{D}} = 0.5$ ms, $n_p = 30$. Simulation results well display that as the number of UE increases, EP increases slowly. In addition, the green curve of the $\kappa - \mu$ shadowed fading ($m = 5$, $\kappa = 4$ and $\mu = 2$) can achieve the same performance as the red curve of the Rician fading ($m = 100$, $\kappa = 8$ and $\mu = 1$). Moreover, we also note that adjusting the values of parameters such as m, κ and μ can feature fading channels that cannot be accommodated by classical models.

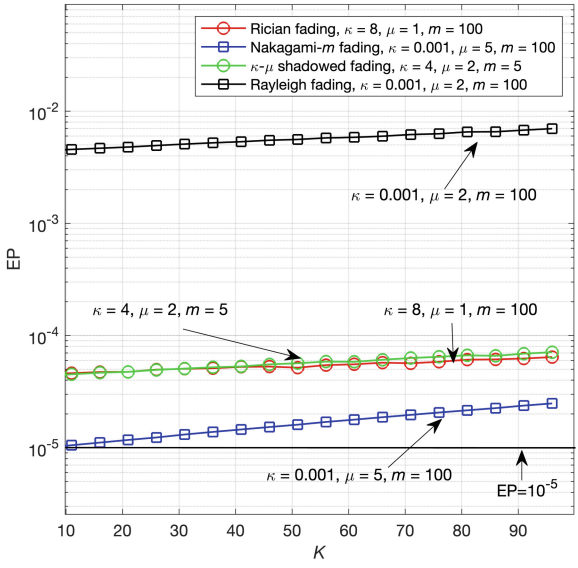

Fig. 5. EP vs. K: $P_u = 30$ dBm, $t_{\mathrm{D}} = 0.5$ ms, $n_p = 30$.

Figure 6 displays the relation between TP and EP for the four classical fading models, when $K = 50$, $t_{\mathrm{D}} = 0.5$ ms, $n_p = 30$. We can see that as the TP increases, the reliability gradually increases. Particularly, when TP is 18 dBm, under the Rician fadin($m = 100$, $\kappa = 8$ and $\mu = 1$), the $\kappa - \mu$ shadowed fading ($m = 5$, $\kappa = 4$ and $\mu = 2$) and the Nakagami-m ($m = 100$, $\kappa = 0.001$ and $\mu = 5$), mURLLC can be enabled. Therefore, when LoP is constrained, we can reduce EP to 10^{-5} by appropriately increasing TP.

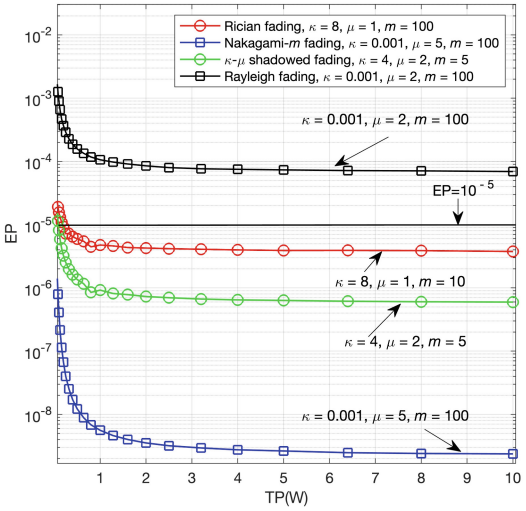

Fig. 6. EP vs. TP: $K = 50$, $t_{\mathrm{D}} = 0.5$ ms, $n_p = 30$.

Figure 7 illustrates the effect of the bandwidth value on the EP under the four classical fading models, when $K = 50$, $t_{\mathrm{D}} = 0.5$ ms, $n_p = 30$. Simulation results well display that as the bandwidth increases, EP decreases gradually. We can see that when B is less than 1080 kHz, CF mMIMO can achieve 99.999% reliability under the Rician fading ($m = 100$, $\kappa = 8$ and $\mu = 1$), the $\kappa - \mu$ shadowed fading ($m = 5$, $\kappa = 4$ and $\mu = 2$) and the Nakagami-m ($m = 100$, $\kappa = 0.001$ and $\mu = 5$). In addition, comparing the red curve and green curve, we can find that the $\kappa - \mu$ shadowed fading has better reliability than the Rician fading with the same parameters.

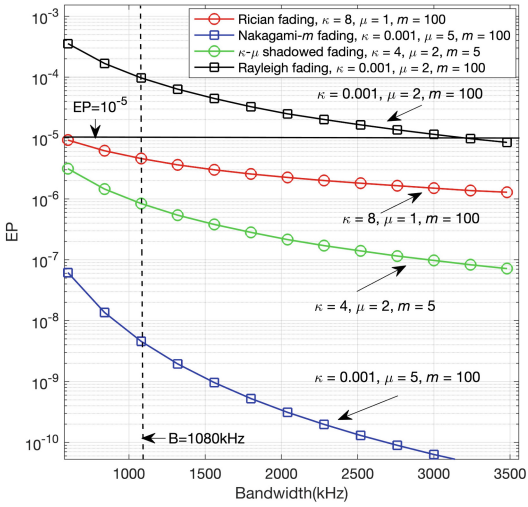

Fig. 7. EP vs. Bandwidth(kHz): $K = 50$, $t_{\mathrm{D}} = 0.5$ ms, $n_p = 30$.

Figure 8 shows the relationship between achievable data rate and SNR under different Latency and EP, when $K = 50$, $n_p = 30$, $P_u = 30$ dBm. We can clearly see that the achievable data rate increases continuously as the SNR. When the achievable data rate of UE is determined, comparing the red curve with the green curve or the blue curve and black curve, the SNR can be increased to meet the requirements of mURLLC.

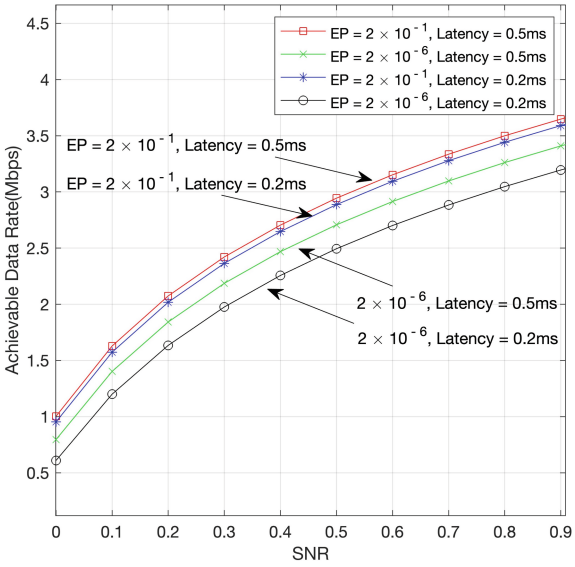

Fig. 8. Achievable Data Rate vs. SNR: $K = 50$, $n_p = 30$, $P_u = 30$ dBm.

6 Conclusion

In the article, based on the CF mMIMO system, we have studied the implementation of mURLLC under $\kappa - \mu$ shadowed fading model. In the UL, we have derived the channel estimation matrix and deduced the PDF of PPSNR. By using the FBL information theory, we have obtained the EP. Further, by applying the GSSA to minimize EP, the optimal LoP has been gained. We have tested the relation among latency, EP, LoP, TP, bandwidth, as well as the number of UE. Then, simulation results well displayed that if the appropriate CF mMIMO system parameters are configured, mURLLC will be enabled. Under the $\kappa - \mu$ shadowed fading model, the conclusion of simulations about mURLLC can be extended to nearly all classic fading models.

References

1. Popovski, P., et al.: Wireless access in ultra-reliable low-latency communication (URLLC). IEEE Trans. Commun. **67**(8), 5783–5801 (2019)
2. Polyanskiy, Y., Poor, H.V., Verdú, S.: Channel coding rate in the finite blocklength regime. IEEE Trans. Inf. Theory **56**(5), 2307–2359 (2010)
3. Nasir, A.A., Tuan, H.D., Ngo, H.Q., Duong, T.Q., Poor, H.V.: Cell-free massive MIMO in the short blocklength regime for URLLC. IEEE Trans. Wireless Commun. **20**(9), 5861–5871 (2021)
4. Ngo, H.Q., Ashikhmin, A., Yang, H., Larsson, E.G., Marzetta, T.L.: Cell-free massive MIMO versus small cells. IEEE Trans. Wireless Commun. **16**(3), 1834–1850 (2017)
5. Ngo, H.Q., Larsson, E.G., Marzetta, T.L.: Energy and spectral efficiency of very large multiuser MIMO systems. IEEE Trans. Commun. **61**(4), 1436–1449 (2013)
6. Zeng, J., Lv, T., Liu, R.P., Su, X., Guo, Y.J., Beaulieu, N.C.: Enabling ultrareliable and low-latency communications under shadow fading by massive MU-MIMO. IEEE Internet Things J. **7**(1), 234–246 (2020)
7. Paris, J.F.: Statistical characterization of $\kappa-\mu$ shadowed fading. IEEE Trans. Veh. Technol. **63**(2), 518–526 (2014)
8. Buzzi, S., D'Andrea, C.: Subspace tracking and least squares approaches to channel estimation in millimeter wave multiuser MIMO. IEEE Trans. Commun. **67**(10), 6766–6780 (2019)
9. Zeng, J., Lv, T., Liu, R.P., Su, X., Beaulieu, N.C., Guo, Y.J.: Linear minimum error probability detection for massive MU-MIMO with imperfect CSI in URLLC. IEEE Trans. Veh. Technol. **68**(11), 11384–11388 (2019)
10. Huan, S., Chao, Z., Jianhua, L.: Analysis of the signal-structure-based MMSE detector for interleaved OFDMA uplink. In: 2009 IEEE Youth Conference on Information, Computing and Telecommunication, pp. 231–234. IEEE, Beijing (2009)
11. Bhatnagar, M.R.: On the sum of correlated squared $\kappa - \mu$ shadowed random variables and its application to performance analysis of MRC. IEEE Trans. Veh. Technol. **64**(6), 2678–2684 (2015)
12. Koh, B., Choi, S., Chun, J.: A SAR autofocus technique with MUSIC and golden section search for range bins with multiple point scatterers. IEEE Geosci. Remote Sens. Lett. **12**(8), 1600–1604 (2015)